

Learning generative models for valid knockoffs using novel multivariate-rank based statistics

Shoaib Bin Masud¹, Shuchin Aeron^{1*}

June 3, 2025

Abstract

We consider the problem of generating valid knockoffs for knockoff filtering which is a statistical method that provides provable false discovery rate guarantees for any model selection procedure. To this end, we are motivated by recent advances in multivariate *distribution-free* goodness-of-fit tests namely, the rank energy (RE), that is derived using theoretical results characterizing the optimal maps in the Monge’s Optimal Transport (OT) problem. However, direct use of RE for learning generative models is not feasible because of its high computational and sample complexity, saturation under large support discrepancy between distributions, and non-differentiability in generative parameters. To alleviate these, we begin by proposing a variant of the RE, dubbed as soft rank energy (sRE), and its kernel variant called as soft rank maximum mean discrepancy (sRMMD) using entropic regularization of Monge’s OT problem. We then use sRMMD to generate deep knockoffs and show via extensive evaluation that it is a novel and effective method to produce valid knockoffs, achieving comparable, or in some cases improved tradeoffs between detection power Vs false discoveries.

1 Introduction

Selection of significant features with control over the false discovery rates (FDR), is one of the most important problems in application of machine learning methods [Jović et al., 2015, Rietschel et al., 2018] for problems such as untargeted metabolomics [Heinemann, 2019] and genome-wide association study (GWAS) [Frommlet et al., 2012]. Due to the large number of features involved, it is of utmost importance to provide provable guarantees in selecting the true underlying features that can explain certain phenotypic conditions.

Classical methods of FDR control depend on the assumptions on how the features and the responses are related [Benjamini and Hochberg, 1995, Gavrilov et al., 2009]. Barber and Candès in their seminal paper [Candès et al., 2016], proposed a novel FDR control approach, called the Model-X knockoff that can be used as a statistical wrapper around any machine learning method that can select features. Model-X knockoff does not rely on the nature of the relationship between the features and responses and therefore is *model-free*. In order to control the FDR, the Model-X framework generates a synthetic set of features called knockoffs, which mimic the original features but are conditionally independent of the responses given the original features.

Related works. Existing methods of knockoff generation either (i) assume the distribution of the features, or (ii) incorporate a generative model to learn the feature distribution from data. Second-order knockoff [Candès et al., 2016] assumes that the distribution of the features is jointly Gaussian. Another knockoff generation

*1 - Tufts University, Dept. of ECE, **Corresponding authors:** Shoaib Bin Masud, email: Shoaib_Bin.Masud@tufts.edu.

approach based on the Hidden Markov Model (HMM) [Sesia et al., 2019] characterizes the feature distribution with the help a Markov chain. Conditional independence knockoff (CIK) [Liu and Rigollet, 2019] can produce valid knockoffs only if the Gaussian graphical model associated with the features is a tree. A more flexible approach that samples knockoffs from a Bayesian network is discussed in [Gimenez et al., 2019], where the covariates are modeled as the observed variables of the network.

Methods such as KnockoffGAN [Salimans et al., 2016], Deep Knockoffs [Romano et al., 2020], and Auto-Encoding knockoff [Liu and Zheng, 2018] focus on learning a deep generative model to produce valid knockoffs. To create valid knockoffs, KnockoffGAN employs a generative adversarial network (GAN) that requires simultaneous training of four different but interconnected neural networks and is therefore computationally expensive. Auto-Encoding knockoff uses latent variables to reconstruct the covariate distribution using a variational autoencoder [Kingma and Welling, 2019]. The performance of this method depends on the dimension of the latent space considered. Higher dimensional latent space can be used to make the model better but may have diminished power if the covariates violate the low-dimensional approximation. Deep-Knockoffs uses the celebrated two-sample goodness-of-fit statistic called maximum mean discrepancy (MMD) [Gretton et al., 2012] as the loss function in a generative model to produce knockoffs. Though training a generative model with MMD is less expensive [Li et al., 2015], in high dimension MMD has less power [Ramdas et al., 2015]. Another method, called DDLK [Sudarshan et al., 2020] generates knockoffs by first maximizing the likelihood of the features and then minimizing the KL (Kullback-Liebler) divergence between the joint distribution of the features and the knockoffs and any possible swaps between them. KL divergence cannot provide a useful gradient when the supports of the two distributions are disjoint [Bińkowski et al., 2018], which is a long-recognized problem for KL divergence-based discrepancy measures.

Summary of main contributions: We introduce a new statistic called soft Rank Energy (sRE), which is heavily inspired by the recent development in *multivariate distribution-free goodness-of-fit tests* based on Rank Energy (RE) [Deb and Sen, 2019], that in turn is based on the fundamental results in optimal transportation theory [McCann et al., 1995]. sRE is the extension of RE that is obtained by entropic regularization of the optimal transport problem. Similar to [Cuturi et al., 2019], this makes sRE, when used as loss function, a differentiable function of the generative model parameters. We highlight on the properties of sRE which make it a desirable candidate for measuring two-sample goodness-of-fit. We also introduce the kernel variant of sRE called soft Rank Maximum Mean Discrepancy (sRMMD). We inspect the behaviour of sRE and sRMMD w.r.t. the sample size, dimensions and the regularization parameters. We show that with an appropriate entropy regularizer, and sample size, sRMMD based generative models do not suffer from mode collapse. We use sRMMD as a loss function in a generative model to produce valid knockoffs. We demonstrate that knockoffs generated by our proposed method can keep the FDR under control, with either comparable or increased detection power compared to existing baselines in the cases considered.

Notations: We use bold-math capital letters \mathbf{X} for multivariate random variables, bold-face capital letters \mathbf{X} for matrices and maps, lower-case bold face bold-math \mathbf{x} for vectors. We denote by $\mathcal{P}(\mathbb{R}^d)$ - the set absolutely continuous measure in \mathbb{R}^d . $\stackrel{d}{=}$ refers to the equality in distribution. $\mathcal{N}(\mu_d, \mathbb{I}_d)$ is referred to as the Gaussian distribution, where \mathbb{I}_d is a d -dimensional identity matrix. The rest of the notations is standard and should be clear from the context.

2 Overview of the knockoff filter

Given that $\mathbf{X} = (X_1, \dots, X_d) \in \mathbb{R}^d$ and $y \in \mathbb{R}$ are the multivariate random variable and the response variable, respectively. Assume that the distribution associated with \mathbf{X} is known and denoted as $F_{\mathbf{X}}$, whereas there exists no knowledge about the conditional distribution, $F_{y|\mathbf{X}}$. A variable X_j is said to be “null or unimportant” *if and only if* y is conditionally independent on X_j , given the other variables, $y \perp\!\!\!\perp X_j | X_{-j}$, where $X_{-j} = \{X_1, \dots, X_d\} \setminus X_j$. Otherwise, it will be considered as a relevant or important variable. Under these assumptions, the primary goal of the Model-X Knockoff filter [Candes et al., 2016] is to discover *as many relevant variables* as possible while keeping the FDR under control. FDR is defined as following,

$$\text{FDR} = \mathbb{E} \left[\frac{|\hat{\mathcal{S}} \cap \mathcal{H}_0|}{\max(1, |\hat{\mathcal{S}}|)} \right],$$

where \mathcal{H}_0 denotes the true set of null or unimportant variables and $\hat{\mathcal{S}} \subseteq \{1, 2, \dots, d\}$ is a subset of variables that is selected by any variable selection method.

To control FDR, Model-X knockoff [Candes et al., 2016] generates knockoff, $\tilde{\mathbf{X}}$ - a random vector that satisfies the following properties:

- (a) **Exchangeability:** $(\mathbf{X}, \tilde{\mathbf{X}})_{\text{swap}(B)} \stackrel{d}{=} (\mathbf{X}, \tilde{\mathbf{X}})$,
- (b) **Conditional independence:** $y \perp\!\!\!\perp \tilde{\mathbf{X}} | \mathbf{X}$.

Exchangeability property ensures that for any subset $B \subset \{1, 2, \dots, p\}$, the joint distribution remains unchanged when the variables and their corresponding knockoffs exchange their positions. That is, for any random vector, $\mathbf{X} = (X_1, X_2, X_3)$, and a set, $B = \{2, 3\}$, in order to satisfy the exchangeability condition, we must have $(X_1, \tilde{X}_2, \tilde{X}_3, \tilde{X}_1, X_2, X_3) \stackrel{d}{=} (X_1, X_2, X_3, \tilde{X}_1, \tilde{X}_2, \tilde{X}_3)$. The second property ensures that knockoffs are generated without the knowledge of the response variable.

To use knockoffs in a controlled variable selection procedure, it is important to construct a knockoff statistic, W_j that can satisfy the *flip-sign* property. That is, $W_j = w_j([\mathbf{X}, \tilde{\mathbf{X}}], y)$, for some function w_j and B , must satisfy the following,

$$w_j([\mathbf{X}, \tilde{\mathbf{X}}]_{\text{swap}(B)}, y) = \begin{cases} w_j([\mathbf{X}, \tilde{\mathbf{X}}], y) & \text{if } j \notin B, \\ -w_j([\mathbf{X}, \tilde{\mathbf{X}}], y) & \text{if } j \in B. \end{cases} \quad (1)$$

Equation (1) says that, swapping the position of j -th variable with its knockoff will change the sign of W_j .

Given the knockoff statistics W_j for $j = 1, \dots, d$, a guaranteed control of FDR is achieved by the knockoff filter at a level $q \in (0, 1)$ by selecting j -th variable, $j \in \{1, \dots, d\}$, such that $W_j \geq \tau$, where τ is achieved via the following,

$$\tau = \min_{t > 0} \left\{ t : \frac{1 + |\{j : W_j \leq -t\}|}{|\{j : W_j \geq t\}|} \leq q \right\}. \quad (2)$$

The power and FDR control of a knockoff filter depends on how the **exchangeability** condition is satisfied. A naive approach called Second-order knockoff [Candes et al., 2016] only approximates first two moments to satisfy the exchangeability condition assuming that the covariates follow a multivariate Gaussian distribution. However, Second-order knockoffs provide insufficient guarantees for FDR control if the assumption does not hold. On the other hand, Deep knockoffs [Romano et al., 2020] use a generative model based on the maximum mean discrepancy (MMD) [Gretton et al., 2012] statistic to produce higher-order knockoffs that can achieve provable FDR guarantee under general conditions.

We now briefly describe the knockoff generation procedure used in Deep Knockoffs [Romano et al., 2020].

2.1 Deep knockoffs

Deep knockoff [Romano et al., 2020] employs a deep neural network, $f_{\theta}(\mathbf{X}, \mathbf{V})$ that generates a knockoff $\tilde{\mathbf{X}} \in \mathbb{R}^d$ from original input variable $\mathbf{X} \in \mathbb{R}^d$, and a noise vector $\mathbf{V} \sim \mathcal{N}(0, \mathbb{I}_d) \in \mathbb{R}^d$. Here, θ denotes the parameters

of the network. In order to satisfy the exchangeability condition without any assumption on the covariate distribution, Deep knockoff [Romano et al., 2020] uses the unbiased MMD [Li et al., 2015] estimate as a loss function- that can match the higher-order moments including the first two moments. In particular, for a design matrix $\mathbf{X} \in \mathbb{R}^{n \times d}$ with n observations, and the corresponding knockoff matrix $\tilde{\mathbf{X}} \in \mathbb{R}^{n \times d}$, Deep knockoff computes the loss in the following manner:

$$\ell_{\text{MMD}}(\mathbf{X}, \tilde{\mathbf{X}}) = \text{MMD}[(\mathbf{X}', \tilde{\mathbf{X}}'), (\tilde{\mathbf{X}}'', \mathbf{X}'')] + \text{MMD}[(\mathbf{X}', \tilde{\mathbf{X}}'), (\mathbf{X}'', \tilde{\mathbf{X}}'')_{\text{swap}(B)}], \quad (3)$$

where $\mathbf{X}', \mathbf{X}'', \tilde{\mathbf{X}}', \tilde{\mathbf{X}}'' \in \mathbb{R}^{n/2 \times d}$ are obtained by randomly splitting the design matrix in half and B is a uniformly chosen random subset of $\{1, \dots, d\}$, such that $j \in B$ with probability $1/2$. To increase the power of the knockoff filter, a regularization term is added to the loss function that penalizes the large pairwise correlation,

$$D_{\text{corr}}(\mathbf{X}, \tilde{\mathbf{X}}) = \|\text{diag}(\hat{\mathbf{G}}_{\mathbf{X}\tilde{\mathbf{X}}}) - 1 + s_{\text{SDP}}^*(\hat{\mathbf{G}}_{\mathbf{X}\mathbf{X}})\|^2, \quad (4)$$

where $\hat{\mathbf{G}}_{\mathbf{X}\tilde{\mathbf{X}}}, \hat{\mathbf{G}}_{\mathbf{X}\mathbf{X}} \in \mathbb{R}^{d \times d}$ are the empirical covariance matrices and s_{SDP}^* is the solution to the following semidefinite programming,

$$s_{\text{SDP}}^*(\Sigma_{\mathbf{X}, \mathbf{X}}) = \arg \min_{s \in [0, 1]^d} \sum_{j=1}^p |1 - s_j|, \quad \text{s.t. } 2\Sigma \succeq \text{diag}(s).$$

Deep knockoffs also adds a second-order loss term (Equation 7 in [Romano et al., 2020]) which is claimed to be effective in reducing the training time. Total loss of the generative model is given as,

$$\ell(\mathbf{X}, \tilde{\mathbf{X}}) = \ell_{\text{MMD}}(\mathbf{X}, \tilde{\mathbf{X}}) + \lambda \ell_{\text{s-o}}(\mathbf{X}, \tilde{\mathbf{X}}) + \delta D_{\text{corr}}(\mathbf{X}, \tilde{\mathbf{X}}). \quad (5)$$

For further insights on the generative model, we refer the reader to [Romano et al., 2020] and reference therein.

3 Background: OT based multivariate rank energy

Rank-based goodness-of-fit tests have been studied comprehensively in 1-D e.g., Kolmogorov-Smirnov test [Smirnov, 1939], Wilcoxon signed-rank test [Wilcoxon, 1947], Wald-Wolfowitz runs test [Wald and Wolfowitz, 1940]. Unlike 1-D, due to the lack of canonical ordering in d - dimensional space, for $d \geq 2$, the notion of rank cannot be defined in a straightforward way. Recently several authors [Hallin et al., 2017, 2021, Chernozhukov et al., 2017, Deb and Sen, 2019, Hallin et al., 2020, Shi et al., 2020b,a] studied the notion of multivariate rank based on OT theory. In this paper, we will consider the setting in [Deb and Sen, 2019] explicitly and build upon the ideas therein.

Ranks and Quantiles for univariate distributions. Let X be a univariate random variable with c.d.f. $F : \mathbb{R} \rightarrow [0, 1]$. It is a standard result that when F is continuous, the random variable $F(X) \sim \text{U}[0, 1]$ - the uniform distribution on $[0, 1]$. For any $x \in \mathbb{R}$, $F(x)$ is referred to as the *rank-function*. For any $0 < p < 1$, the *quantile function* is defined by $Q(p) = \inf\{x \in \mathbb{R} : p \leq F(x)\}$. When F is continuous, the quantile function $Q = F^{-1}$.

Ranks and Quantiles for multivariate distributions. Since there exists no natural ordering in \mathbb{R}^d , defining ranks and quantiles in high dimension is not straightforward. To extend the notion of rank in \mathbb{R}^d , theory of Optimal Transport (OT) has been used to propose meaningful and useful notions of multivariate rank and quantile functions [Hallin et al., 2017, Chernozhukov et al., 2017, Deb and Sen, 2019, Hallin et al., 2020]. In it's most standard-setting, given two distributions, a source distribution $\mu \in \mathcal{P}(\mathbb{R}^d)$ and a target distribution $\nu \in \mathcal{P}(\mathbb{R}^d)$, OT aims to find a map $\mathbf{T} : \mathbb{R}^d \rightarrow \mathbb{R}^d$ that pushes μ to ν with a minimal cost. That is, given $\mathbf{X} \sim \mu$,

and $\mathbf{Y} \sim \nu$, OT finds a map \mathbf{T} ,

$$\inf_{\mathbf{T}} \int \|\mathbf{x} - \mathbf{T}(\mathbf{x})\|^2 d\mu(\mathbf{x}) \text{ subject to. } \mathbf{Y} = \mathbf{T}(\mathbf{X}) \sim \nu. \quad (6)$$

Note that if $\mathbf{T}(\mathbf{X}) \sim \nu$ when $\mathbf{X} \sim \mu$, we write $\nu = \mathbf{T}_{\#}\mu$. The *key insight* in using the theory of OT to multivariate ranks and quantiles comes from noticing that in case of $d = 1$, the optimal transport map is given by $\mathbf{T} = F_{\nu}^{-1} \circ F_{\mu}$, where F_{μ} and F_{ν} are the distribution functions for μ and ν , respectively. When $\nu = \mathbf{U}[0, 1]$, this gives the rank function F_{μ} . Following [Deb and Sen, 2019], McCann's theorem [McCann et al., 1995] stated below, is used to extend the notion of rank to the multivariate setting.

Theorem 1 ([McCann et al., 1995]). *Assume $\mu, \nu \in \mathcal{P}(\mathbb{R}^d)$ be absolutely continuous measures, then there exists transport maps $\mathbf{R}(\cdot)$ and $\mathbf{Q}(\cdot)$, that are gradients of real-valued d -variate convex functions such that $\mathbf{R}_{\#}\mu = \nu$, $\mathbf{Q}_{\#}\nu = \mu$, \mathbf{R} and \mathbf{Q} are unique and $\mathbf{R} \circ \mathbf{Q}(\mathbf{X}) = \mathbf{X}$, $\mathbf{Q} \circ \mathbf{R}(\mathbf{Y}) = \mathbf{Y}$.*

Based on this result, the authors in [Deb and Sen, 2019] give the following definitions for the rank and quantile functions in high dimensions.

Definition 1 ([Deb and Sen, 2019]). *Given an absolutely continuous measure $\mu \in \mathcal{P}(\mathbb{R}^d)$ and $\nu = \mathbf{U}[0, 1]^d$ - the uniform measure on the unit cube in \mathbb{R}^d , the ranks and quantile maps for μ are defined as the maps $\mathbf{R}(\cdot)$ and $\mathbf{Q}(\cdot)$, respectively as defined in Theorem 1.*

3.1 Rank Energy

To state the definition of Rank Energy [Deb and Sen, 2019], we begin with a brief introduction on the Energy distance [Baringhaus and Franz, 2004, Székely and Rizzo, 2013]. Energy distance is a multivariate, two-sample goodness-of-fit measure. Given two independent multivariate random variables $\mathbf{X} \in \mathbb{R}^d \sim \mu_{\mathbf{X}}$, $\mathbf{Y} \in \mathbb{R}^d \sim \mu_{\mathbf{Y}}$, where $\mu_{\mathbf{X}}, \mu_{\mathbf{Y}} \in \mathcal{P}(\mathbb{R}^d)$, energy distance is defined via:

$$E(\mathbf{X}, \mathbf{Y}) = \gamma_d \int_{\mathbb{R}} \int_{\mathcal{S}^{d-1}} \left(\mathbb{P}(\mathbf{a}^{\top} \mathbf{X} \leq t) - \mathbb{P}(\mathbf{a}^{\top} \mathbf{Y} \leq t) \right)^2 d\kappa(\mathbf{a}) dt, \quad (7)$$

where $\gamma = (2\Gamma(d/2))^{-1} \sqrt{\pi}(d-1)\Gamma((d-1)/2)$ for $d > 1$, $\mathcal{S}^{d-1} \doteq \{\mathbf{x} \in \mathbb{R}^d : \|\mathbf{x}\| = 1\}$, and $\kappa(\cdot)$ denotes the uniform measure on \mathcal{S}^{d-1} . It is self-evident that for all $\mathbf{a} \in \mathcal{S}^{d-1}$ and $t \in \mathbb{R}$, the two measures will be equal *if and only if* $\mathbb{P}(\mathbf{a}^{\top} \mathbf{X} \leq t) = \mathbb{P}(\mathbf{a}^{\top} \mathbf{Y} \leq t)$.

Deb [Deb and Sen, 2019] proposed a rank-based version of the energy measure and defined it as the rank energy measure.

Definition 2 ([Deb and Sen, 2019]). *Suppose that $\mathbf{X} \sim \mu_{\mathbf{X}}$ and $\mathbf{Y} \sim \mu_{\mathbf{Y}}$. Let \mathbf{R}_{λ} denote the population rank corresponding to a mixture distribution, $\lambda\mu_{\mathbf{X}} + (1 - \lambda)\mu_{\mathbf{Y}}$, for some $\lambda \in (0, 1)$. Then the population rank energy RE_{λ} is defined as:*

$$\text{RE}_{\lambda}(\mathbf{X}, \mathbf{Y}) = \gamma_d \int_{\mathbb{R}} \int_{\mathcal{S}^{d-1}} \left(\mathbb{P}(\mathbf{a}^{\top} \mathbf{R}_{\lambda}(\mathbf{X}) \leq t) - \mathbb{P}(\mathbf{a}^{\top} \mathbf{R}_{\lambda}(\mathbf{Y}) \leq t) \right)^2 d\kappa(\mathbf{a}) dt. \quad (8)$$

In other words, rank energy between \mathbf{X} and \mathbf{Y} is the energy measure between the corresponding ranks, $\mathbf{R}_{\lambda}(\mathbf{X})$ and $\mathbf{R}_{\lambda}(\mathbf{Y})$.

$\text{RE}_{\lambda}(\cdot, \cdot)$ is a distribution-free multivariate two-sample goodness-of-fit measure. A nice feature of RE_{λ} is that, in 1-D, it is equivalent to the widely used Cramér-Von Mises [Anderson, 1962] statistic for two-sample distribution testing, [Deb and Sen, 2019].

$$\frac{1}{2} \text{RE}_{\lambda}(X, Y) = \int (F_X(t) - F_Y(t))^2 dH_{\lambda}(t), \quad (9)$$

where F_X, F_Y and H_λ are absolutely continuous distribution functions corresponding to the probability measures μ_X, μ_Y and $\lambda\mu_X + (1 - \lambda)\mu_Y$, respectively. Based on this result, we note the following lemma.

Lemma 1. *Let μ_X and μ_Y are supported on the interval $[a, b]$ and $[a + s, b + s]$, respectively, and their mixture measure denoted as $\mu_H = \lambda\mu_X + (1 - \lambda)\mu_Y$, for any $\lambda \in (0, 1)$. Also, let F_X, F_Y and H_λ , denote the cumulative distribution functions for μ_X, μ_Y and μ_H , respectively. Then RE_λ as a function of s , is a constant independent of s for $s \geq b - a$ and $s \leq a - b$.*

Proof. Please see Supplementary A.1. □

We also verify this phenomenon empirically for higher dimensions in Section 5.

Sample rank energy. To define sample rank energy (hereafter referred to as RE), we begin with the definition of a sample rank map. Given a set of i.i.d. samples $\{\mathbf{X}_1, \dots, \mathbf{X}_m\} \in \mathbb{R}^d$ with empirical measure $\mu_m^{\mathbf{X}} = m^{-1} \sum_{i=1}^m \delta_{\mathbf{X}_i}$ and a set of Halton sequence $\mathcal{H}_m^d := \{\mathbf{h}_1, \dots, \mathbf{h}_m\} \subset [0, 1]^d$ [Deb and Sen, 2019] with empirical measure $\nu_m^{\mathbf{H}} = m^{-1} \sum_{i=1}^m \delta_{\mathbf{h}_i}$ that weakly converges to $\text{U}[0, 1]^d$, to compute a sample rank map $\hat{\mathbf{R}}_m$, one solves for the following discrete optimal transport problem,

$$\hat{\mathbf{P}} = \arg \min_{\mathbf{P} \in \Pi} \sum_{i,j=1}^m \mathbf{C}_{i,j} \mathbf{P}_{i,j}, \quad (10)$$

where $\mathbf{C}_{i,j} = \|\mathbf{X}_i - \mathbf{h}_j\|^2$, $\Pi = \{\mathbf{P} : \mathbf{P}\mathbf{1} = \frac{1}{m}\mathbf{1}, \mathbf{1}^\top \mathbf{P} = \frac{1}{m}\mathbf{1}^\top\}$. It is well known that the solution to this problem, under the given set-up, is one of the scaled permutation matrices. Consequently, one obtains a map $\hat{\mathbf{R}}_m(\mathbf{X}_i) = \mathbf{h}_{\sigma(i)}$, where $\sigma(i)$ is the non-zero index in the i -th row of $\hat{\mathbf{P}}$.

Now to compute RE between two sets of i.i.d. samples $\{\mathbf{X}_1, \dots, \mathbf{X}_m\} \sim \mu_m^{\mathbf{X}}$ and $\{\mathbf{Y}_1, \dots, \mathbf{Y}_n\} \sim \mu_n^{\mathbf{Y}}$, a joint sample rank map $\hat{\mathbf{R}}_{m,n}$ is computed via solving (10) between the joint empirical measure $\mu_{m,n}^{\mathbf{X},\mathbf{Y}} = (m+n)^{-1}(m\mu_m^{\mathbf{X}} + n\mu_n^{\mathbf{Y}})$ and the target empirical measure $\nu_{m,n}^{\mathbf{H}} = (m+n)^{-1} \sum_{i=1}^{m+n} \delta_{\mathbf{h}_i}$. Given the sample ranks corresponding to \mathbf{X}_i 's and \mathbf{Y}_j 's, RE is defined as,

$$\begin{aligned} \text{RE} \doteq & \frac{2}{mn} \sum_{i=1}^m \sum_{j=1}^n \|\hat{\mathbf{R}}_{m,n}(\mathbf{X}_i) - \hat{\mathbf{R}}_{m,n}(\mathbf{Y}_j)\| - \frac{1}{m^2} \sum_{i,j=1}^m \|\hat{\mathbf{R}}_{m,n}(\mathbf{X}_i) - \hat{\mathbf{R}}_{m,n}(\mathbf{X}_j)\| \\ & - \frac{1}{n^2} \sum_{i,j=1}^n \|\hat{\mathbf{R}}_{m,n}(\mathbf{Y}_i) - \hat{\mathbf{R}}_{m,n}(\mathbf{Y}_j)\|. \end{aligned} \quad (11)$$

RE is distribution-free under the null for fixed sample size. However, discrete OT (11) has large sample complexity $\mathcal{O}(n^{-1/d})$ [Genevay et al., 2019] and also computationally expensive $\mathcal{O}(n^3 \log(n))$, given the sample size n . Moreover, RE is constant in the region where the supports of the two distributions are completely disjoint (see Supplementary).

4 Proposed soft rank energy

Towards developing the notion of soft rank energy we first state the Kantorovich relaxation of the Monge problem, where instead of a map, one seeks an optimal coupling π between a source distribution $\mu \in \mathcal{P}(\mathbb{R}^d)$ and a target distribution $\nu \in \mathcal{P}(\mathbb{R}^d)$. That is, given $\mathbf{X} \sim \mu$ and $\mathbf{Y} \sim \nu$, Kantorovich relaxation [Santambrogio, 2015] solves for,

$$\arg \min_{\pi \in \Pi(\mu, \nu)} \int c(\mathbf{x}, \mathbf{y}) d\pi(\mathbf{x}, \mathbf{y}), \quad (12)$$

where $\Pi(\mu, \nu)$ is the set of joint probability measure over the product set $\mathbb{R}^d \times \mathbb{R}^d$ with marginals μ and ν , and typically $c(\mathbf{x}, \mathbf{y})$ is a symmetric positive cost function satisfying $c(\mathbf{x}, \mathbf{x}) = 0$. It is well-known that the Kantorovich solution coincides with the Monge solution, whenever the latter exists [Santambrogio, 2015].

Adding an entropic regularization term to (12) allows one to get the transport plan in closed form [Feydy et al., 2019] and makes the OT problem differentiable everywhere w.r.t. the weights of the input measures [Blondel et al., 2018]. For any regularizer $\varepsilon > 0$, the primal formulation of the entropy regularized OT is given by:

$$\arg \min_{\pi \in \Pi(\mu, \nu)} \int c(\mathbf{x}, \mathbf{y}) d\pi(\mathbf{x}, \mathbf{y}) + \varepsilon \text{KL}(\pi(\mathbf{x}, \mathbf{y}) | \mu(\mathbf{x}) \otimes \nu(\mathbf{y})), \quad (13)$$

$$\text{where } \text{KL}(\pi(\mathbf{x}, \mathbf{y}) | \mu(\mathbf{x}) \otimes \nu(\mathbf{y})) \doteq \int \ln \left(\frac{d\pi(\mathbf{x}, \mathbf{y})}{d\mu(\mathbf{x})d\nu(\mathbf{y})} \right) d\pi(\mathbf{x}, \mathbf{y}).$$

The unconstrained dual of (13) is achieved by using the Fenchel-Rockafellar's duality theorem [Clason et al., 2021],

$$\arg \max_{f, g} \int f(\mathbf{x}) d\mu(\mathbf{x}) + \int g(\mathbf{y}) d\nu(\mathbf{y}) - \varepsilon \int \int \exp\left(\frac{1}{\varepsilon}(f(\mathbf{x}) + g(\mathbf{y}) - c(\mathbf{x}, \mathbf{y}))\right) d\mu(\mathbf{x}) d\nu(\mathbf{y}) + \varepsilon, \quad (14)$$

where (f, g) is a pair of continuous functions. Given the optimal dual solutions f, g , the optimal plan π^ε is given as [Seguy et al., 2017],

$$d\pi^\varepsilon(\mathbf{x}, \mathbf{y}) = \exp\left(\frac{1}{\varepsilon}(f(\mathbf{x}) + g(\mathbf{y}) - c(\mathbf{x}, \mathbf{y}))\right) d\mu(\mathbf{x}) d\nu(\mathbf{y}).$$

Unlike \mathbf{T} , π^ε is not a map, but a *diffused coupling*, where the degree of diffusion is directly proportional to ε . Given π^ε , we now define the soft rank.

Definition 3. Given an absolutely continuous measure $\mu \in \mathcal{P}(\mathbb{R}^d)$ and $\nu = \text{U}[0, 1]^d$ - the uniform measure on the unit cube in \mathbb{R}^d , the soft rank is defined as:

$$\mathbf{R}^\varepsilon(\mathbf{x}) \doteq \int_{\mathbf{y}} \frac{\mathbf{y} d\pi^\varepsilon(\mathbf{x}, \mathbf{y})}{\int_{\mathbf{y}} d\pi^\varepsilon(\mathbf{x}, \mathbf{y})}. \quad (15)$$

In other words, soft rank $\mathbf{R}^\varepsilon(\cdot)$ is the conditional expectation of \mathbf{y} under π^ε , given $\mathbf{X} = \mathbf{x}$.

We note that the soft rank as defined above corresponds to what is referred to as the barycentric projection of optimal transport plan [Seguy et al., 2017, Deb et al., 2021]. Based on Definition 3, we now define the population version of soft rank energy.

Definition 4. Given two independent multivariate random variables $\mathbf{X} \sim \mu_{\mathbf{X}}$ and $\mathbf{Y} \sim \mu_{\mathbf{Y}}$, where $\mu_{\mathbf{X}}, \mu_{\mathbf{Y}} \in \mathcal{P}(\mathbb{R}^d)$. Also, let $\mathbf{R}_\lambda^\varepsilon$ denote the population soft rank corresponding to a mixture distribution $\lambda\mu_{\mathbf{X}} + (1 - \lambda)\mu_{\mathbf{Y}}$, for some $\lambda \in (0, 1)$. Then the population soft rank energy is defined as:

$$\text{sRE}_\lambda^\varepsilon(\mathbf{X}, \mathbf{Y}) = \gamma_d \int_{\mathbb{R}} \int_{\mathcal{S}^{d-1}} \left(\mathbb{P}(\mathbf{a}^\top \mathbf{R}_\lambda^\varepsilon(\mathbf{X}) \leq t) - \mathbb{P}(\mathbf{a}^\top \mathbf{R}_\lambda^\varepsilon(\mathbf{Y}) \leq t) \right)^2 d\kappa(\mathbf{a}) dt. \quad (16)$$

In other words, soft rank energy is the energy measure between the soft ranks corresponding to \mathbf{X} and \mathbf{Y} .

Based on this definition, we state the following lemma.

Lemma 2. Under the assumptions of Definition 4, we state the following properties of $\text{sRE}_\lambda^\varepsilon$.

(a) Given $\mathbf{X}_1, \mathbf{X}_2$ i.i.d. $\sim \mu_{\mathbf{X}}$ and given $\mathbf{Y}_1, \mathbf{Y}_2$ i.i.d. $\sim \mu_{\mathbf{Y}}$, following [Székely and Rizzo, 2013], the soft rank energy as defined via equation (16) is equivalent to

$$\text{sRE}_\lambda^\varepsilon(\mathbf{X}_1, \mathbf{Y}_1) = 2\mathbb{E}\|\mathbf{R}_\lambda^\varepsilon(\mathbf{X}_1) - \mathbf{R}_\lambda^\varepsilon(\mathbf{Y}_1)\| - \mathbb{E}\|\mathbf{R}_\lambda^\varepsilon(\mathbf{X}_1) - \mathbf{R}_\lambda^\varepsilon(\mathbf{X}_2)\| - \mathbb{E}\|\mathbf{R}_\lambda^\varepsilon(\mathbf{Y}_1) - \mathbf{R}_\lambda^\varepsilon(\mathbf{Y}_2)\|. \quad (17)$$

(b) (Symmetric) $\text{sRE}_\lambda^\varepsilon(\mathbf{X}_1, \mathbf{Y}_1) = \text{sRE}_\lambda^\varepsilon(\mathbf{Y}_1, \mathbf{X}_1)$,

(c) $\text{sRE}_\lambda^\varepsilon(\mathbf{X}_1, \mathbf{Y}_1) = 0$ if $\mathbf{X}_1 \stackrel{d}{=} \mathbf{Y}_1$,

(d) $\text{sRE}_\lambda^\varepsilon$ will converge to RE_λ as $\varepsilon \rightarrow 0$.

Proof. Please see Supplementary A.2. □

Note that one has the flexibility to employ any multivariate *two-sample test* to measure the goodness-of-fit between distributions. That is, in similar fashion, one can define RMMD_λ or $\text{sRMMD}_\lambda^\varepsilon$ by measuring the maximum mean discrepancy (MMD) [Gretton et al., 2012] between the rank-transformed random variables $\mathbf{R}_\lambda(\mathbf{X})$ and $\mathbf{R}_\lambda(\mathbf{Y})$ or $\mathbf{R}_\lambda^\varepsilon(\mathbf{X})$ and $\mathbf{R}_\lambda^\varepsilon(\mathbf{Y})$.

We now state the sample soft rank energy (sRE $^\varepsilon$) and sample soft rank maximum mean discrepancy (sRMMD $^\varepsilon$). For the sake of brevity, hereafter, we refer to them as sRE and sRMMD, respectively.

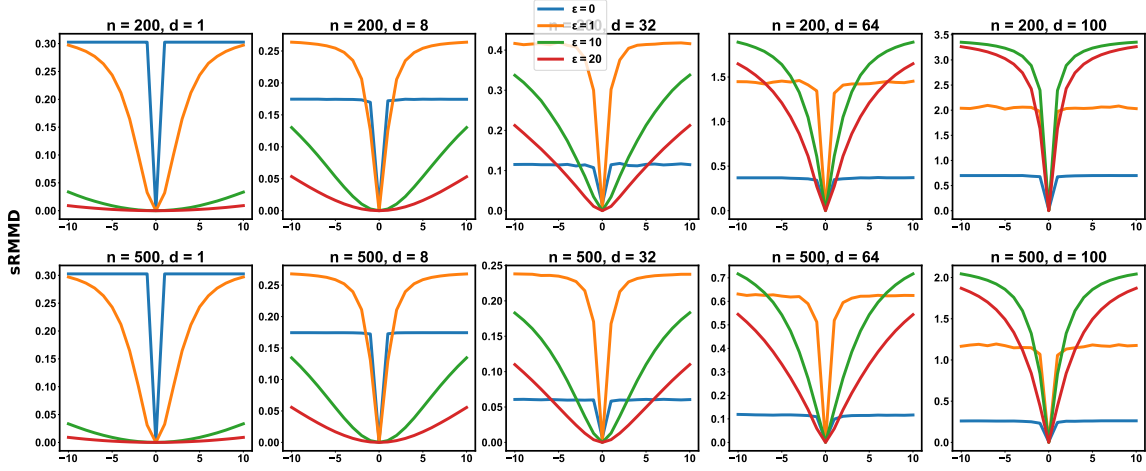


Figure 1: $\text{RMMD}(\varepsilon = 0)$ and sRMMD (y-axis) between two uniform distributions with bounded supports. n and d denote the number of samples and dimension. RMMD achieves a constant maximum in the region, where the two supports are completely disjoint, for all n, d . sRMMD do not saturate for increased d if ε and n is larger.

4.1 sRE and sRMMD

Using the similar setting as described in Section 3.1, we now define the sample soft rank map $\hat{\mathbf{R}}_m^\varepsilon$. To compute $\hat{\mathbf{R}}_m^\varepsilon$, first an entropy regularized OT is solved via Sinkhorn [Peyré et al., 2019]-a *iterative fixed point* algorithm for an entropy regularizer, $\varepsilon > 0$,

$$\mathbf{P}^\varepsilon = \arg \min_{\mathbf{P} \in \Pi} \sum_{i,j=1}^m \mathbf{C}_{i,j} \mathbf{P}_{i,j} - \varepsilon H(\mathbf{P}), \quad (18)$$

where $\mathbf{C}_{i,j} = \|\mathbf{X}_i - \mathbf{h}_j\|^2$, $\Pi = \{\mathbf{P} : \mathbf{P}\mathbf{1} = \frac{1}{m}\mathbf{1}, \mathbf{1}^\top \mathbf{P} = \frac{1}{m}\mathbf{1}^\top\}$, and $H(\mathbf{P}) = -\sum_{i,j} \mathbf{P}_{i,j} \log \mathbf{P}_{i,j}$ is the entropy functional. Given \mathbf{P}^ε , sample soft rank map is defined via,

$$\hat{\mathbf{R}}_m^\varepsilon(\mathbf{X}_i) = \sum_{j=1}^m \frac{\mathbf{P}_{i,j}^\varepsilon}{\sum_{j=1}^m \mathbf{P}_{i,j}^\varepsilon} \mathbf{h}_j. \quad (19)$$

Now, to define sRE and sRMMD, we first compute a joint sample soft rank map $\hat{\mathbf{R}}_{m,n}^\varepsilon$ via solving (18) between $\mu_{m,n}^{\mathbf{X},\mathbf{Y}}$ and $\nu_{m,n}^{\mathbf{H}}$. Given the sample soft ranks corresponding to \mathbf{X}_i 's and \mathbf{Y}_j 's, we define sRE as,

$$\begin{aligned} \text{sRE} \doteq & \frac{2}{mn} \sum_{i=1}^m \sum_{j=1}^n \|\hat{\mathbf{R}}_{m,n}^\varepsilon(\mathbf{X}_i) - \hat{\mathbf{R}}_{m,n}^\varepsilon(\mathbf{Y}_j)\| - \frac{1}{m^2} \sum_{i,j=1}^m \|\hat{\mathbf{R}}_{m,n}^\varepsilon(\mathbf{X}_i) - \hat{\mathbf{R}}_{m,n}^\varepsilon(\mathbf{X}_j)\| \\ & - \frac{1}{n^2} \sum_{i,j=1}^n \|\hat{\mathbf{R}}_{m,n}^\varepsilon(\mathbf{Y}_i) - \hat{\mathbf{R}}_{m,n}^\varepsilon(\mathbf{Y}_j)\| \end{aligned} \quad (20)$$

and sRMMD, with a characteristic kernel function $k(\cdot, \cdot)$, as,

$$\begin{aligned} \text{sRMMD} \doteq & \frac{1}{m(m-1)} \sum_{i,j \neq i}^m k(\widehat{\mathbf{R}}_{m,n}^\epsilon(\mathbf{X}_i), \widehat{\mathbf{R}}_{m,n}^\epsilon(\mathbf{X}_j)) - \frac{2}{mn} \sum_{i,j=1}^{m,n} k(\widehat{\mathbf{R}}_{m,n}^\epsilon(\mathbf{X}_i), \widehat{\mathbf{R}}_{m,n}^\epsilon(\mathbf{Y}_j)) \\ & + \frac{1}{n(n-1)} \sum_{i,j \neq i}^n k(\widehat{\mathbf{R}}_{m,n}^\epsilon(\mathbf{Y}_i), \widehat{\mathbf{R}}_{m,n}^\epsilon(\mathbf{Y}_j)), \end{aligned} \quad (21)$$

Employing entropic OT to define rank maps make sRE and sRMMD differentiable everywhere [Seguy et al., 2017]. Use of Sinkhorn iterations [Peyré et al., 2019] allows one to exploit the power of GPU. The computational complexity of entropic OT is $\mathcal{O}(\varepsilon^{-2} n^2 \log n \|\mathbf{C}\|_\infty^2)$ [Peyré et al., 2019] and with increasing ε , complexity decreases. Moreover, under some mild assumptions, namely sub-Gaussianity of the measures, the estimation of entropic OT does not suffer from the curse of dimensionality for a sufficiently large ε [Mena and Niles-Weed, 2019].

4.2 Proposed Knockoff generation

We now propose to use sRMMD as the loss function in a generative model to produce knockoffs. Given the design matrix $\mathbf{X} \in \mathbb{R}^{n \times d}$ and its knockoff matrix $\tilde{\mathbf{X}} \in \mathbb{R}^{n \times d}$, the loss function is defined via,

$$\ell(\mathbf{X}, \tilde{\mathbf{X}}) = \ell_{\text{sRMMD}}(\mathbf{X}, \tilde{\mathbf{X}}) + \lambda \ell_{\text{s-o}}(\mathbf{X}, \tilde{\mathbf{X}}) + \delta \text{D}_{\text{corr}}(\mathbf{X}, \tilde{\mathbf{X}}). \quad (22)$$

$\ell_{\text{sRMMD}}(\mathbf{X}, \tilde{\mathbf{X}})$ is computed in a similar way as (3),

$$\ell_{\text{sRMMD}}(\mathbf{X}, \tilde{\mathbf{X}}) = \text{sRMMD}[(\mathbf{X}', \tilde{\mathbf{X}}'), (\tilde{\mathbf{X}}'', \mathbf{X}'')] + \text{sRMMD}[(\mathbf{X}', \tilde{\mathbf{X}}'), (\mathbf{X}'', \tilde{\mathbf{X}}'')_{\text{swap}(S)}].$$

For optimal performance, the hyperparameters should be tuned to the specific data distribution at hand.

5 Experiments

In this section, we empirically observe the properties of sRMMD as a loss function and evaluate the performance of the proposed knockoff generation method on synthetic and real datasets.

sRMMD as a loss function. To investigate the quality of sRMMD as a loss function in a generative model, we consider two Uniform distributions having bounded supports, $\text{U}[0, 1]^d$ and $\text{U}[s, s+1]^d$ and measure the sRMMD between them for $s \in [-10, 10]$. Figure 1 empirically shows the saturation behavior of sRMMD.

This saturation limits the use of sRMMD for learning a generative model, as the saturation in those regimes will imply vanishing gradients for learning. As one can see from the plots that either higher values of ε or larger sample size is needed with increasing dimensions in order to prevent the saturation behavior of sRMMD. Plots showing similar behavior for sRE can be found in Supplementary C.2.

sRMMD for a generative model. To check this, we sample $\mathbf{X} \sim \sum_{k=1}^3 m_k \mathcal{N}(\mu_k, \Sigma_k)$, which is a Gaussian mixture model with three modes. Σ_k is a d -dimensional covariance matrix whose (i, j) entry is $\rho^{|i-k|}$. We use $(\rho_1, \rho_2, \rho_3) = (0.6, 0.4, 0.2)$, cluster mean $(\mu_1, \mu_2, \mu_3) = (0, 20, 40)$ and mixture proportion $(m_1, m_2, m_3) = (0.4, 0.2, 0.4)$ for $d = 16$. We use (22) with $(\lambda, \gamma) = (0, 0)$ in the generative model described in [Romano et al., 2020].

Figure 2 shows that the generative model suffers from mode collapse for $\varepsilon = 1$, which is expected (Figure 1). On the other hand, $\varepsilon = 5, 10$, perfectly captures the mode, covariance, and proportions of the Gaussian mixture model, hence establish sRMMD as a suitable loss function for the knockoff generation.

Synthetic dataset. We evaluate the performance of sRMMD based knockoffs on four different distributional settings adapted from [Romano et al., 2020]. Below, we briefly describe each setting with the optimal

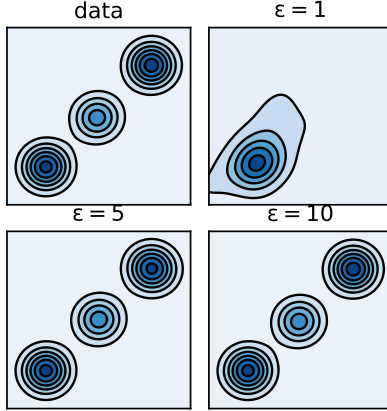


Figure 2: Mode reconstruction for a Gaussian mixture model (upper left) with sRMMD for various ε

hyperparameters used in (22) to train the model.

- (a) *Multivariate Gaussian*: An AR(1) model, with $\mathbf{X} = (X_1, X_2, \dots, X_d) \sim \mathcal{N}(0, \Sigma)$, where Σ - a d dimensional covariance matrix, whose (i, j) entry is $\rho^{|i-j|}$. ρ is set to 0.5. Hyperparameters (λ, δ) were set to $(1, 1)$ in the loss function (22).
- (b) *Gaussian Mixture Model*: Mixture of three multivariate Gaussian distributions, $\mathcal{N}(0, \Sigma_1)$, $\mathcal{N}(0, \Sigma_2)$ and $\mathcal{N}(0, \Sigma_3)$, each of equal probability. $\Sigma_1, \Sigma_2, \Sigma_3$ have the same first-order autoregressive structure. Covariance matrices are $\Sigma_1 = 0.3^{|i-j|}$, $\Sigma_2 = 0.5^{|i-j|}$, and $\Sigma_3 = 0.7^{|i-j|}$. $(\lambda, \delta) = (1, 1)$.
- (c) *Multivariate Student's t distribution*: $\mathbf{X} = \sqrt{\frac{(\nu-2)}{\nu}} \frac{\mathbf{Z}}{\sqrt{\Gamma}}$, where $\nu = 3$ is the degrees of freedom, $\mathbf{Z} \sim \mathcal{N}(0, \Sigma)$ and Γ is independently drawn from a Gamma distribution with shape and rate parameters both equal to $\nu/2$. $(\lambda, \delta) = (1, 0.1)$.
- (d) *Sparse Gaussian Variables*: For a scalar random variable $\eta \sim \mathcal{N}(0, 1)$, and random subset $A \in \{1, \dots, p\}$ of size $|A| = L$, sparse Gaussian variable is defined as,

$$X_j = \sqrt{\frac{\binom{L}{p}}{\binom{L-1}{p-1}}} \begin{cases} \eta, & \text{if } j \in A, \\ 0, & \text{otherwise} \end{cases}$$

$$\text{and, } \Sigma_{i,j} = \begin{cases} 1, & \text{if } i = j, \\ \frac{L-1}{p-1} & \text{otherwise.} \end{cases}$$

with $L = 30$, and $(\lambda, \delta) = (1, 5)$.

Experimental setup: We consider a fully connected neural network with 6 hidden layers, each consists of $5d$ nodes as the generative architecture. This architecture is almost similar to the structure used in [Romano et al., 2020]. The network takes $\mathbf{X} \in \mathbb{R}^d$ and a noise vector $V \in \mathbb{R}^d \sim \mathcal{N}(\mathbf{0}, \mathbb{I}_d)$ as inputs and produce the knockoff vector $\tilde{\mathbf{X}} \in \mathbb{R}^d$. For further insights, we refer the reader to [Romano et al., 2020].

We train the model with Stochastic gradient descent with $n = 2500$ training samples, each of $d = 100$ dimension. The minibatch size, learning rate and the number of epochs were set to 500, 0.01, and 100, respectively. We use $\varepsilon = 10$, to compute the soft ranks. We employ a Gaussian mixture kernel $k(x, y) = \frac{1}{8} \sum_{i=1}^8 \exp[-\|x - y\|_2^2 / (2\sigma^2)]$, with $\sigma = (1, 2, 4, 8, 16, 32, 64, 128)$ to compute sRMMD.

We design a matrix $\mathbf{X} \in \mathbb{R}^{m \times d}$, with $m = 100$ random samples unknown to the training dataset and generate knockoffs $\tilde{\mathbf{X}} \in \mathbb{R}^{m \times d}$. For each sample $i \in \{1, 2, \dots, m\}$, we simulate the response according to a Gaussian linear

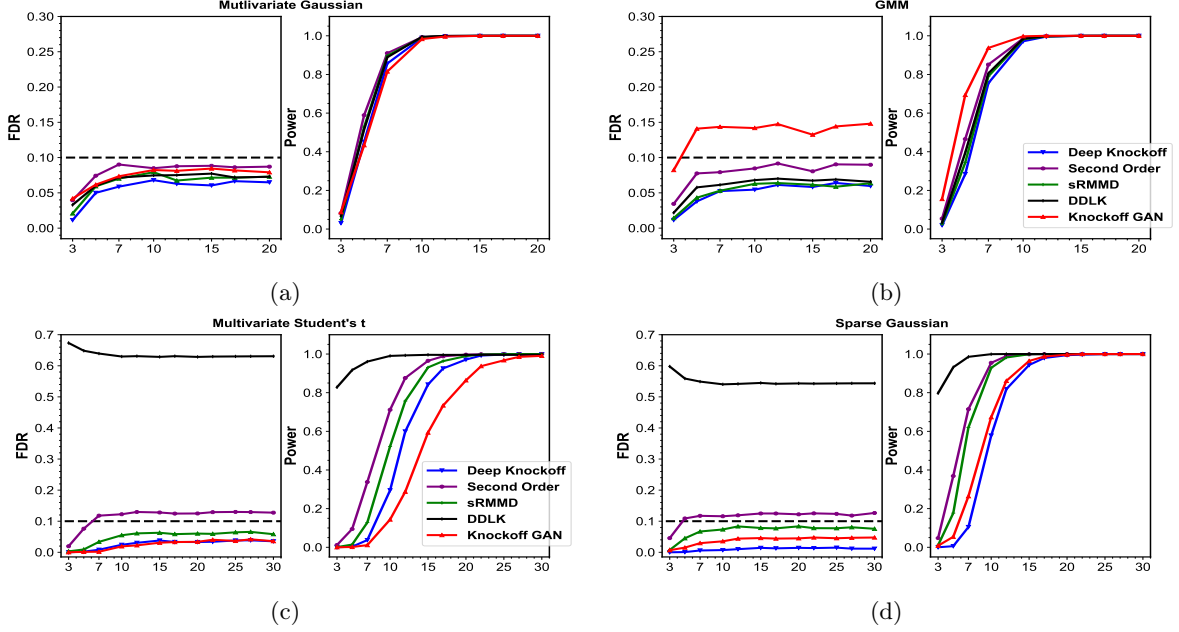


Figure 3: FDR vs amplitude and power vs. amplitude. FDR level is set to 0.1 (black dotted line).

model, $y_i = \mathbf{X}_i^\top \boldsymbol{\beta} + z$, where $z \sim \mathcal{N}(0, 1)$. $\boldsymbol{\beta} \in \mathbb{R}^d$ denotes the coefficient vector which has 30 non-zero entries each having an amplitude equal to a/\sqrt{m} . To find the knockoff statistics, we fit a LASSO-regression [Friedman et al., 2010] model on the augmented matrix $[\mathbf{X}, \tilde{\mathbf{X}}] \in \mathbb{R}^{m \times 2d}$ with the response vector $\mathbf{y} \in \mathbb{R}^m$ and compute the coefficients $[\hat{\boldsymbol{\beta}}, \hat{\boldsymbol{\beta}}^K] \in \mathbb{R}^{2d}$ via solving,

$$(\hat{\boldsymbol{\beta}}, \hat{\boldsymbol{\beta}}^K) = \arg \min_{(\boldsymbol{\beta}, \boldsymbol{\beta}^K)} \frac{1}{2m} \|\mathbf{y} - \mathbf{X}\boldsymbol{\beta} - \tilde{\mathbf{X}}\boldsymbol{\beta}^K\|_2^2 + \alpha(\|\boldsymbol{\beta}\|_1 + \|\boldsymbol{\beta}^K\|_1), \quad (23)$$

where $\hat{\boldsymbol{\beta}}$ and $\hat{\boldsymbol{\beta}}^K$ denotes the coefficient vectors corresponding to the original variables and the knockoffs, respectively, and α is a hyperparameter chosen carefully for each distributional setting. Absolute LASSO coefficient difference is taken as the knockoff statistics, $W_j = |\hat{\beta}_j| - |\hat{\beta}_j^k|$, for each $j \in \{1, \dots, d\}$. We apply (2) on the statistics W_j for the FDR level $q = 0.1$. We repeat the experiment 500 times for different values of a and take the average FDR and power.

We compare our method to other knockoff generation techniques, namely Second-order knockoff [Candes et al., 2016], Deep Knockoffs [Romano et al., 2020], KnockoffGAN [Jordon et al., 2018] and DDLK [Sudarshan et al., 2020]. For all comparisons, we use publicly available implementations of the code (if available) and used their recommended configurations and hyperparameters. For each method, we follow the exact procedure to compute knockoff statistics as described above.

Performance on synthetic data. Figure 3 shows the average FDR vs. amplitude and power vs. amplitude curves for different knockoff generation methods. For the multivariate Gaussian distribution, we observe that, all methods showcase very similar power and FDR control over the entire amplitude region. For the Gaussian mixture model, KnockoffGAN shows higher power, but cannot control the FDR, whereas sRMMMD and other methods demonstrate comparable power and keep the FDR below the FDR level. We notice that for the multivariate Student’s t distribution, Second-order and DDLK knockoffs achieves comparably higher power in the low amplitude region but fail to control the FDR. We also observe that, though KnockoffGAN and Deep

knockoffs can control the FDR but they have low power in the small amplitude region. On the other hand, sRMMD gains higher power than the KnockoffGAN and Deep knockoff at this region and is also able to control the FDR. For the sparse Gaussian setting, we notice that DDLK gains very high power in the small amplitude region, but has poor control over FDR. Second-order knockoff also fails to control the FDR in this case. On the other hand, the plot indicates that knockoffGAN and Deep knockoff control the FDR but have less power in the small amplitude region, whereas sRMMD gains higher power and more control over the FDR in this region.

Evaluation on real data benchmark We apply the proposed knockoff filter to a publicly available metabolomics dataset in order to discover important biomarkers. In absence of the ground truth, to qualitatively analyze the performance, we cross-reference the selected metabolites with published literature. We use a study titled *Longitudinal Metabolomics of the Human Microbiome in Inflammatory Bowel Disease* [Lloyd-Price et al., 2019] which is available at the NIH’s common Fund’s National Metabolomics Data Repository (NMDR) website, the Metabolomics Workbench, <https://www.metabolomicsworkbench.org/> under the project DOI: 10.21228/M82T15. The study is related to Inflammatory Bowel Disease (IBD), that describes the conditions like ulcerative colitis (UC) and Crohn’s disease (CD). We use *C18 Reverse-Phase negative mode* dataset which was collected under this study. There are 546 samples in this dataset, each having 91 metabolites on average. Each sample belongs to one of the three different classes e.g., CD, UC, non-IBD and we assign response y to either $\{0, 1, \text{or } 2\}$, respectively. Before applying the knockoff filter, we preprocess the dataset in multiple steps, (i) keeping the metabolites that have at least 80% filled values (ii) missing value imputation using K-nearest neighbour (KNN) [Gromski et al., 2014] (iii) standardization. After generating the knockoffs, we apply Random Forest classifier [Trainor et al., 2017] on the augmented matrix, and take the difference between the out-of-bag (OOB) [Trainor et al., 2017] scores corresponding to the original and knockoffs as the knockoff statistics. We repeat the whole procedure 100 times, since the generated knockoffs are random. We select those metabolites that appear at least 70 times out of 100 instances, setting the FDR level at 0.05. 22 metabolites are found as significant. Among them 19 metabolites are shown to have relation to IBD, which are cross referenced by published literature.

Additional experiments and the list of the selected metabolites are to be found in Supplementary C, and, B.

6 Conclusion and Future work

In this paper, we introduced a new statistic called soft-rank Maximum Mean Discrepancy (sRMMD) and used it to generate valid knockoffs. We demonstrate through a series of experiments that sRMMD is a valid loss function that can be used in a generative model. We also showed that knockoffs generated using the proposed method have better power and FDR control on synthetic datasets sampled from Gaussian and non-Gaussian distributional settings. While the proposed approach is better than several existing methods for knockoff generation, it is still computationally expensive compared to MMD. An important future work is to characterize in a precise manner the behaviour of sRMMD w.r.t. the sample size, dimension, and the entropy regularizer.

7 Acknowledgement

This research was sponsored by the U.S. Army DEVCOM Soldier Center, and was accomplished under Cooperative Agreement Number W911QY-19-2-0003. The views and conclusions contained in this document are those of the authors and should not be interpreted as representing the official policies, either expressed or implied, of the U.S. Army DEVCOM Soldier Center, or the U.S. Government. The U. S. Government

is authorized to reproduce and distribute reprints for Government purposes notwithstanding any copyright notation hereon.

We also acknowledge support from the U.S. National Science Foundation under award HDR-1934553 for the Tufts T-TRIPODS Institute. Shuchin Aeron is also supported in part by NSF CCF:1553075, NSF RAISE 1931978, NSF ERC planning 1937057, and AFOSR FA9550-18-1-0465.

References

- T. W. Anderson. On the distribution of the two-sample cramer-von mises criterion. *The Annals of Mathematical Statistics*, pages 1148–1159, 1962.
- L. Baringhaus and C. Franz. On a new multivariate two-sample test. *Journal of multivariate analysis*, 88(1): 190–206, 2004.
- C. Bauset, L. Gisbert-Ferrándiz, and J. Cosín-Roger. Metabolomics as a promising resource identifying potential biomarkers for inflammatory bowel disease. *Journal of Clinical Medicine*, 10(4):622, 2021.
- Y. Benjamini and Y. Hochberg. Controlling the false discovery rate: a practical and powerful approach to multiple testing. *Journal of the Royal statistical society: series B (Methodological)*, 57(1):289–300, 1995.
- M. Bińkowski, D. J. Sutherland, M. Arbel, and A. Gretton. Demystifying mmd gans. *arXiv preprint arXiv:1801.01401*, 2018.
- M. Blondel, V. Seguy, and A. Rolet. Smooth and sparse optimal transport. In *International Conference on Artificial Intelligence and Statistics*, pages 880–889. PMLR, 2018.
- E. Candes, Y. Fan, L. Janson, and J. Lv. Panning for gold: Model-x knockoffs for high-dimensional controlled variable selection. *arXiv preprint arXiv:1610.02351*, 2016.
- R. Caprilli, M. Cesarini, E. Angelucci, and G. Frieri. The long journey of salicylates in ulcerative colitis: The past and the future. *Journal of Crohn’s and Colitis*, 3(3):149–156, 2009.
- G. Carlier, V. Duval, G. Peyré, and B. Schmitzer. Convergence of entropic schemes for optimal transport and gradient flows. *SIAM Journal on Mathematical Analysis*, 49(2):1385–1418, 2017.
- V. Chernozhukov, A. Galichon, M. Hallin, M. Henry, et al. Monge–kantorovich depth, quantiles, ranks and signs. *Annals of Statistics*, 45(1):223–256, 2017.
- C. Clason, D. A. Lorenz, H. Mahler, and B. Wirth. Entropic regularization of continuous optimal transport problems. *Journal of Mathematical Analysis and Applications*, 494(1):124432, 2021.
- M. Cuturi, O. Teboul, and J.-P. Vert. Differentiable ranks and sorting using optimal transport. *arXiv preprint arXiv:1905.11885*, 2019.
- N. Deb and B. Sen. Multivariate rank-based distribution-free nonparametric testing using measure transportation. *arXiv preprint arXiv:1909.08733*, 2019.
- N. Deb, P. Ghosal, and B. Sen. Rates of estimation of optimal transport maps using plug-in estimators via barycentric projections. *arXiv preprint arXiv:2107.01718*, 2021.

- J. Feydy, T. Séjourné, F.-X. Vialard, S.-i. Amari, A. Trouvé, and G. Peyré. Interpolating between optimal transport and mmd using sinkhorn divergences. In *The 22nd International Conference on Artificial Intelligence and Statistics*, pages 2681–2690. PMLR, 2019.
- D. Fretland, D. Widomski, S. Levin, and T. Gaginella. Colonic inflammation in the rabbit induced by phorbol-12-myristate-13-acetate. *Inflammation*, 14(2):143–150, 1990.
- J. Friedman, T. Hastie, and R. Tibshirani. Regularization paths for generalized linear models via coordinate descent. *Journal of statistical software*, 33(1):1, 2010.
- F. Frommlet, F. Ruhaltinger, P. Twaróg, and M. Bogdan. Modified versions of bayesian information criterion for genome-wide association studies. *Computational Statistics & Data Analysis*, 56(5):1038–1051, 2012.
- Y. Gavrilov, Y. Benjamini, and S. K. Sarkar. An adaptive step-down procedure with proven fdr control under independence. *The Annals of Statistics*, 37(2):619–629, 2009.
- A. Genevay, L. Chizat, F. Bach, M. Cuturi, and G. Peyré. Sample complexity of sinkhorn divergences. In *The 22nd International Conference on Artificial Intelligence and Statistics*, pages 1574–1583. PMLR, 2019.
- J. R. Gimenez, A. Ghorbani, and J. Zou. Knockoffs for the mass: new feature importance statistics with false discovery guarantees. In *The 22nd International Conference on Artificial Intelligence and Statistics*, pages 2125–2133. PMLR, 2019.
- A. Gretton, K. M. Borgwardt, M. J. Rasch, B. Schölkopf, and A. Smola. A kernel two-sample test. *The Journal of Machine Learning Research*, 13(1):723–773, 2012.
- P. S. Gromski, Y. Xu, H. L. Kotze, E. Correa, D. I. Ellis, E. G. Armitage, M. L. Turner, and R. Goodacre. Influence of missing values substitutes on multivariate analysis of metabolomics data. *Metabolites*, 4(2):433–452, 2014.
- M. Hallin, D. Hlubinka, and Š. Hudecová. Fully distribution-free center-outward rank tests for multiple-output regression and manova. *arXiv preprint arXiv:2007.15496*, 2020.
- M. Hallin, E. del Barrio, J. Cuesta-Albertos, and C. Matrán. Distribution and quantile functions, ranks and signs in dimension d: A measure transportation approach. *The Annals of Statistics*, 49(2):1139–1165, 2021.
- M. Hallin et al. On distribution and quantile functions, ranks and signs in rd. *ECARES Working Papers*, 2017.
- J. Heinemann. Machine learning in untargeted metabolomics experiments. In *Microbial Metabolomics*, pages 287–299. Springer, 2019.
- J. Jordon, J. Yoon, and M. van der Schaar. Knockoffgan: Generating knockoffs for feature selection using generative adversarial networks. In *International Conference on Learning Representations*, 2018.
- A. Jović, K. Brkić, and N. Bogunović. A review of feature selection methods with applications. In *2015 38th international convention on information and communication technology, electronics and microelectronics (MIPRO)*, pages 1200–1205. Ieee, 2015.
- D. P. Kingma and J. Ba. Adam: A method for stochastic optimization. *arXiv preprint arXiv:1412.6980*, 2014.
- D. P. Kingma and M. Welling. Auto-encoding variational bayes. *arXiv preprint arXiv:1312.6114*, 2013.

- D. P. Kingma and M. Welling. An introduction to variational autoencoders. *arXiv preprint arXiv:1906.02691*, 2019.
- F. Kuroki, M. Iida, T. Matsumoto, K. Aoyagi, K. Kanamoto, and M. Fujishima. Serum n3 polyunsaturated fatty acids are depleted in crohn’s disease. *Digestive diseases and sciences*, 42(6):1137–1141, 1997.
- A. Lavelle and H. Sokol. Gut microbiota-derived metabolites as key actors in inflammatory bowel disease. *Nature Reviews Gastroenterology & Hepatology*, 17(4):223–237, 2020.
- G. Le Gall, S. O. Noor, K. Ridgway, L. Scovell, C. Jamieson, I. T. Johnson, I. J. Colquhoun, E. K. Kemsley, and A. Narbad. Metabolomics of fecal extracts detects altered metabolic activity of gut microbiota in ulcerative colitis and irritable bowel syndrome. *Journal of proteome research*, 10(9):4208–4218, 2011.
- T. Lee, T. Clavel, K. Smirnov, A. Schmidt, I. Lagkouvardos, A. Walker, M. Lucio, B. Michalke, P. Schmitt-Kopplin, R. Fedorak, et al. Oral versus intravenous iron replacement therapy distinctly alters the gut microbiota and metabolome in patients with ibd. *Gut*, 66(5):863–871, 2017.
- S. R. Levan, K. A. Stamnes, D. L. Lin, A. R. Panzer, E. Fukui, K. McCauley, K. E. Fujimura, M. McKean, D. R. Ownby, E. M. Zoratti, et al. Elevated faecal 12, 13-dihome concentration in neonates at high risk for asthma is produced by gut bacteria and impedes immune tolerance. *Nature microbiology*, 4(11):1851–1861, 2019.
- Y. Li, K. Swersky, and R. Zemel. Generative moment matching networks. In *International Conference on Machine Learning*, pages 1718–1727. PMLR, 2015.
- J. Liu and P. Rigollet. Power analysis of knockoff filters for correlated designs. *arXiv preprint arXiv:1910.12428*, 2019.
- Y. Liu and C. Zheng. Auto-encoding knockoff generator for fdr controlled variable selection. *arXiv preprint arXiv:1809.10765*, 2018.
- J. Lloyd-Price, C. Arze, A. N. Ananthakrishnan, M. Schirmer, J. Avila-Pacheco, T. W. Poon, E. Andrews, N. J. Ajami, K. S. Bonham, C. J. Brislawn, et al. Multi-omics of the gut microbial ecosystem in inflammatory bowel diseases. *Nature*, 569(7758):655–662, 2019.
- R. J. McCann et al. Existence and uniqueness of monotone measure-preserving maps. *Duke Mathematical Journal*, 80(2):309–324, 1995.
- G. Mena and J. Niles-Weed. Statistical bounds for entropic optimal transport: Sample complexity and the central limit theorem. *Advances in Neural Information Processing Systems*, 32, 2019.
- G. Peyré, M. Cuturi, et al. Computational optimal transport: With applications to data science. *Foundations and Trends® in Machine Learning*, 11(5-6):355–607, 2019.
- N. D. Price, A. T. Magis, J. C. Earls, G. Glusman, R. Levy, C. Lausted, D. T. McDonald, U. Kusebauch, C. L. Moss, Y. Zhou, et al. A wellness study of 108 individuals using personal, dense, dynamic data clouds. *Nature biotechnology*, 35(8):747, 2017.
- X. Qin. Etiology of inflammatory bowel disease: a unified hypothesis. *World journal of gastroenterology: WJG*, 18(15):1708, 2012.
- A. Ramdas, S. J. Reddi, B. Póczos, A. Singh, and L. A. Wasserman. On the decreasing power of kernel and distance based nonparametric hypothesis tests in high dimensions. In *AAAI*, 2015.

- C. Rietschel, J. Yoon, and M. van der Schaar. Feature selection for survival analysis with competing risks using deep learning. *arXiv preprint arXiv:1811.09317*, 2018.
- Y. Romano, M. Sesia, and E. Candès. Deep knockoffs. *Journal of the American Statistical Association*, 115(532):1861–1872, 2020.
- S. Saber, R. M. Khalil, W. S. Abdo, D. Nassif, and E. El-Ahwany. Olmesartan ameliorates chemically-induced ulcerative colitis in rats via modulating $\text{nf}\kappa\text{b}$ and nrf-2/ho-1 signaling crosstalk. *Toxicology and applied pharmacology*, 364:120–132, 2019.
- T. Salimans, I. Goodfellow, W. Zaremba, V. Cheung, A. Radford, and X. Chen. Improved techniques for training gans. *arXiv preprint arXiv:1606.03498*, 2016.
- F. Santambrogio. Optimal transport for applied mathematicians. *Birkäuser, NY*, 55(58-63):94, 2015.
- V. Seguy, B. B. Damodaran, R. Flamary, N. Courty, A. Rolet, and M. Blondel. Large-scale optimal transport and mapping estimation. *arXiv preprint arXiv:1711.02283*, 2017.
- M. Sesia, C. Sabatti, and E. J. Candès. Gene hunting with hidden markov model knockoffs. *Biometrika*, 106(1):1–18, 2019.
- H. Shi, M. Drton, and F. Han. Distribution-free consistent independence tests via center-outward ranks and signs. *Journal of the American Statistical Association*, pages 1–16, 2020a.
- H. Shi, M. Hallin, M. Drton, and F. Han. Rate-optimality of consistent distribution-free tests of independence based on center-outward ranks and signs. *arXiv preprint arXiv:2007.02186*, 2020b.
- S. Sitkin and J. Pokrotnieks. Alterations in polyunsaturated fatty acid metabolism and reduced serum eicosadienoic acid level in ulcerative colitis: is there a place for metabolomic fatty acid biomarkers in ibd? *Digestive diseases and sciences*, 63(9):2480–2481, 2018.
- N. V. Smirnov. On the estimation of the discrepancy between empirical curves of distribution for two independent samples. *Bull. Math. Univ. Moscou*, 2(2):3–14, 1939.
- T. Solakivi, K. Kaukinen, T. Kunnas, T. Lehtimäki, M. Mäki, and S. T. Nikkari. Serum fatty acid profile in subjects with irritable bowel syndrome. *Scandinavian journal of gastroenterology*, 46(3):299–303, 2011.
- M. Sudarshan, W. Tansey, and R. Ranganath. Deep direct likelihood knockoffs. *arXiv preprint arXiv:2007.15835*, 2020.
- G. J. Székely and M. L. Rizzo. Energy statistics: A class of statistics based on distances. *Journal of statistical planning and inference*, 143(8):1249–1272, 2013.
- P. J. Trainor, A. P. DeFilippis, and S. N. Rai. Evaluation of classifier performance for multiclass phenotype discrimination in untargeted metabolomics. *Metabolites*, 7(2):30, 2017.
- A. Volkova and K. V. Ruggles. Predictive metagenomic analysis of autoimmune disease identifies robust autoimmunity and disease specific microbial signatures. *Frontiers in microbiology*, 12:418, 2021.
- A. Wald and J. Wolfowitz. On a test whether two samples are from the same population. *The Annals of Mathematical Statistics*, 11(2):147–162, 1940.
- F. Wilcoxon. Probability tables for individual comparisons by ranking methods. *Biometrics*, 3(3):119–122, 1947.

A PROOFS

A.1 Proof of Lemma 1

Proof. To prove this lemma, using slight abuse of notations, we assume that μ_X, μ_Y are supported on $[a, b]$, and μ_Y^s is the shifted measure defined through $\mu_Y^s[T] = \mu_Y[T - s]$, where $s \in \mathbb{R}$, T is any measurable set and $T - s = \{t - s : t \in T\}$. Let $\mu_H^s = \lambda\mu_X + (1 - \lambda)\mu_Y^s$ for any $\lambda \in (0, 1)$, denote the mixture measure. Also let F_X, F_Y and F_Y^s denote the cumulative distribution functions of μ_X, μ_Y and μ_Y^s , respectively, where for any $r \in \mathbb{R}$, by construction $F_Y^s(r) = F_Y(r - s)$.

Now suppose $s \in (-\infty, a - b] \cup [b - a, \infty) = S$. Then we must have,

$$[a, b] \cap [a + s, b + s] \subset \{a, b\}.$$

Now, for all $s \in S$, we have,

$$\begin{aligned} \frac{1}{2} \text{RE}_\lambda(X, Y^s) &= \int_{-\infty}^{\infty} (F_X(t) - F_Y^s(t))^2 dH_\lambda^s(t) \\ &= \int_{-\infty}^{\min(a, a+s)} (F_X(t) - F_Y^s(t))^2 dH_\lambda^s(t) + \int_{\min(a, a+s)}^{\max(b, b+s)} (F_X(t) - F_Y^s(t))^2 dH_\lambda^s(t) + \int_{\max(b, b+s)}^{\infty} (F_X(t) - F_Y^s(t))^2 dH_\lambda^s(t) \\ &= \int_{\min(a, a+s)}^{\max(b, b+s)} (F_X(t) - F_Y^s(t))^2 dH_\lambda^s(t). \end{aligned}$$

Case I: $s \leq a - b$,

$$\begin{aligned} \frac{1}{2} \text{RE}_\lambda(X, Y^s) &= \int_{a+s}^{b+s} (F_Y^s(t) - F_X(t))^2 dH_\lambda^s(t) + \int_{b+s}^a (F_Y^s(t) - F_X(t))^2 dH_\lambda^s(t) + \int_a^b (F_Y^s(t) - F_X(t))^2 dH_\lambda^s(t) \\ &= (1 - \lambda) \int_{a+s}^{b+s} (F_Y^s(t))^2 d\mu_Y^s(t) + 0 + \lambda \int_a^b (1 - F_X(t))^2 d\mu_X(t) \\ &= (1 - \lambda) \int_{a+s}^{b+s} (F_Y(t - s))^2 d\mu_Y(t - s) + \lambda \int_a^b (1 - F_X(t))^2 d\mu_X(t) [\text{assuming absolute continuity}] \\ &= (1 - \lambda) \int_a^b (F_Y(t))^2 d\mu_Y(t) + \lambda \int_a^b (1 - F_X(t))^2 d\mu_X(t), \end{aligned}$$

which is independent of s .

Case II: $a - b \leq s \leq 0$;

$$\begin{aligned} \frac{1}{2} \text{RE}_\lambda(X, Y^s) &= \int_{a+s}^a (F_Y^s(t))^2 dH_\lambda^s(t) + \int_a^{b+s} (F_Y^s(t) - F_X(t))^2 dH_\lambda^s(t) + \int_{b+s}^b (1 - F_X(t))^2 dH_\lambda^s(t) \\ &= (1 - \lambda) \int_{a+s}^a (F_Y^s(t))^2 d\mu_Y^s(t) + \int_a^{b+s} (F_Y^s(t) - F_X(t))^2 (\lambda d\mu_X(t) + (1 - \lambda) d\mu_Y^s(t)) + \lambda \int_{b+s}^b (1 - F_X(t))^2 d\mu_X(t) \end{aligned}$$

this decreases as s moves towards 0.

Case III: $0 \leq s \leq b - a$;

$$\begin{aligned} \frac{1}{2} \text{RE}_\lambda(X, Y^s) &= \int_a^{a+s} (F_X(t))^2 dH_\lambda^s(t) + \int_{a+s}^b (F_X(t) - F_Y^s(t))^2 dH_\lambda^s(t) + \int_b^{b+s} (1 - F_Y^s(t))^2 dH_\lambda^s(t) \\ &= \lambda \int_a^{a+s} (F_X(t))^2 d\mu_X(t) + \int_{a+s}^b (F_X(t) - F_Y^s(t))^2 (\lambda d\mu_X(t) + (1 - \lambda) d\mu_Y^s(t)) + (1 - \lambda) \int_b^{b+s} (1 - F_Y^s(t))^2 d\mu_Y^s(t) \end{aligned}$$

this increases as s moves towards $b - a$.

Case IV : $s \geq b - a$;

$$\begin{aligned}
\frac{1}{2} \text{RE}_\lambda(X, Y^s) &= \int_a^b (\mathbb{F}_X(t) - \mathbb{F}_Y^s(t))^2 d\mathbb{H}_\lambda^s(t) + \int_b^{a+s} (\mathbb{F}_X(t) - \mathbb{F}_Y^s(t))^2 d\mathbb{H}_\lambda^s(t) + \int_{a+s}^{b+s} (\mathbb{F}_X(t) - \mathbb{F}_Y^s(t))^2 d\mathbb{H}_\lambda^s(t) \\
&= \lambda \int_a^b (\mathbb{F}_X(t))^2 d\mu_X(t) + 0 + (1 - \lambda) \int_{a+s}^{b+s} (1 - \mathbb{F}_Y^s(t))^2 d\mu_Y^s(t) \\
&= \lambda \int_a^b (\mathbb{F}_X(t))^2 d\mu_X(t) + (1 - \lambda) \int_{a+s}^{b+s} (1 - \mathbb{F}_Y^s(t - s))^2 d\mu_Y(t - s) [\text{assuming absolute continuity}] \\
&= \lambda \int_a^b (\mathbb{F}_X(t))^2 d\mu_X(t) + (1 - \lambda) \int_a^b (1 - \mathbb{F}_Y(t))^2 d\mu_Y(t),
\end{aligned}$$

which is independent of s .

A.2 Proof of Lemma 2

Proof. (a) Using Lemmas 2.2, 2.3 from [Baringhaus and Franz, 2004], for $\mathbf{X}_1, \mathbf{X}_2 \stackrel{i.i.d.}{\sim} \mu_{\mathbf{X}}$, and $\mathbf{Y}_1, \mathbf{Y}_2 \stackrel{i.i.d.}{\sim} \mu_{\mathbf{Y}}$, we have, □

$$\begin{aligned}
2\mathbb{E}\|\mathbf{X}_1 - \mathbf{Y}_1\| - \mathbb{E}\|\mathbf{X}_1 - \mathbf{X}_2\| - \mathbb{E}\|\mathbf{Y}_1 - \mathbf{Y}_2\| \\
= \gamma_d \int_{\mathcal{S}^{d-1}} \int_{\mathbb{R}} \left(\mathbb{P}(\mathbf{a}^\top \mathbf{X}_1 \leq t) - P(\mathbf{a}^\top \mathbf{Y}_1 \leq t) \right)^2 d\kappa(\mathbf{a}) dt, \tag{24}
\end{aligned}$$

where $\gamma = (2\Gamma(d/2))^{-1} \sqrt{\pi}(d-1)\Gamma((d-1)/2)$ for $d > 1$, $\mathcal{S}^{d-1} = \{\mathbf{x} \in \mathbb{R}^d : \|\mathbf{x}\| = 1\}$, $\mathbf{a} \in \mathcal{S}^{d-1}$, and $\kappa(\cdot)$ denotes the uniform measure on \mathcal{S}^{d-1} . Since, $\mathbf{R}_\lambda^\varepsilon(\mathbf{X}_1)$, $\mathbf{R}_\lambda^\varepsilon(\mathbf{X}_2)$, $\mathbf{R}_\lambda^\varepsilon(\mathbf{Y}_1)$, and $\mathbf{R}_\lambda^\varepsilon(\mathbf{Y}_2)$ denote the transformed multivariate random variables corresponds to $\mathbf{X}_1, \mathbf{X}_2, \mathbf{Y}_1$ and \mathbf{Y}_2 , respectively, we can write the following,

$$\begin{aligned}
2\mathbb{E}\|\mathbf{R}_\lambda^\varepsilon(\mathbf{X}_1) - \mathbf{R}_\lambda^\varepsilon(\mathbf{Y}_1)\| - \mathbb{E}\|\mathbf{R}_\lambda^\varepsilon(\mathbf{X}_1) - \mathbf{R}_\lambda^\varepsilon(\mathbf{X}_2)\| - \mathbb{E}\|\mathbf{R}_\lambda^\varepsilon(\mathbf{Y}_1) - \mathbf{R}_\lambda^\varepsilon(\mathbf{Y}_2)\| \\
= \gamma_d \int_{\mathcal{S}^{d-1}} \int_{\mathbb{R}} \left(\mathbb{P}(\mathbf{a}^\top \mathbf{R}_\lambda^\varepsilon(\mathbf{X}_1) \leq t) - \mathbb{P}(\mathbf{a}^\top \mathbf{R}_\lambda^\varepsilon(\mathbf{Y}_1) \leq t) \right)^2 d\kappa(\mathbf{a}) dt. \tag{25}
\end{aligned}$$

(b) Following the definition of $\text{sRE}_\lambda^\varepsilon(\cdot, \cdot)$,

$$\begin{aligned}
\text{sRE}_\lambda^\varepsilon(\mathbf{X}_1, \mathbf{Y}_1) &= \gamma_d \int_{\mathbb{R}} \int_{\mathcal{S}^{d-1}} \left(\mathbb{P}(\mathbf{a}^\top \mathbf{R}_\lambda^\varepsilon(\mathbf{X}_1) \leq t) - \mathbb{P}(\mathbf{a}^\top \mathbf{R}_\lambda^\varepsilon(\mathbf{Y}_1) \leq t) \right)^2 d\kappa(\mathbf{a}) dt \\
&= \gamma_d \int_{\mathbb{R}} \int_{\mathcal{S}^{d-1}} \left(\mathbb{P}(\mathbf{a}^\top \mathbf{R}_\lambda^\varepsilon(\mathbf{Y}_1) \leq t) - \mathbb{P}(\mathbf{a}^\top \mathbf{R}_\lambda^\varepsilon(\mathbf{X}_1) \leq t) \right)^2 d\kappa(\mathbf{a}) dt \\
&= \text{sRE}_\lambda^\varepsilon(\mathbf{Y}_1, \mathbf{X}_1). \tag{26}
\end{aligned}$$

(c) Assuming $\mathbf{X}_1 \stackrel{d}{=} \mathbf{Y}_1$, we have $\mathbb{P}(\mathbf{a}^\top \mathbf{X}_1 \leq t) = \mathbb{P}(\mathbf{a}^\top \mathbf{Y}_1 \leq t)$ for all $\mathbf{a} \in \mathcal{S}^{d-1}$ and $t \in \mathbb{R}$. Given the rank transformed random variables $\mathbf{R}_\lambda^\varepsilon(\mathbf{X}_1)$, $\mathbf{R}_\lambda^\varepsilon(\mathbf{Y}_1)$ corresponding to \mathbf{X}_1 and \mathbf{Y}_1 , we have $\mathbf{a}^\top \mathbf{R}_\lambda^\varepsilon(\mathbf{X}_1) \stackrel{d}{=} \mathbf{a}^\top \mathbf{R}_\lambda^\varepsilon(\mathbf{Y}_1)$. Therefore, $\text{sRE}_\lambda^\varepsilon(\mathbf{X}_1, \mathbf{Y}_1) = 0$, if $\mathbf{X}_1 \stackrel{d}{=} \mathbf{Y}_1$.

(d) The unique minimizer $\boldsymbol{\pi}^\varepsilon$ converges to the optimal Monge-Kantorovich solution $\boldsymbol{\pi}$ with cost function $c(\cdot) = \|\mathbf{x} - \mathbf{y}\|^p$ [Carlier et al., 2017],

$$\lim_{\varepsilon \rightarrow 0} \boldsymbol{\pi}^\varepsilon \rightarrow \boldsymbol{\pi}, \tag{27}$$

where \rightarrow denotes convergence w.r.t. the weak topology. According to the proposition 2.18 in [Carlier et al., 2017], we have,

$$\lim_{\varepsilon \rightarrow 0} \int_{\mathbf{y}} \mathbf{y} d\boldsymbol{\pi}^\varepsilon(\mathbf{y}|\mathbf{x}) \rightarrow \int_{\mathbf{y}} \mathbf{y} d\boldsymbol{\pi}(\mathbf{y}|\mathbf{x}), \tag{28}$$

which implies that as $\varepsilon \rightarrow 0$, $\mathbf{R}_\lambda^\varepsilon(\cdot)$ will converge to $\mathbf{R}_\lambda(\cdot)$ w.r.t. the weak topology. Consequently, $\text{sRE}_\lambda^\varepsilon(\mathbf{X}_1, \mathbf{Y}_1)$ will converge to $\text{RE}_\lambda(\mathbf{X}_1, \mathbf{Y}_1)$ as $\varepsilon \rightarrow 0$. □

B List of metabolites discovered using the proposed method

Here, we list the metabolites that are found at least 70 times out of 100 instances of knockoffs generated from the real data using the proposed method. We add the references (if found) for the selected metabolites.

Table 1: Metabolites selected at an FDR level ≤ 0.05 . “-” denotes either metabolites are not related to IBD or not found in literature as potential biomarkers.

METABOLITES	REFERENCES
1.2.3.4-tetrahydro- -beta-carboline- -1.3-dicarboxylate	[Volkova and Ruggles, 2021]
Urobilin	[Lloyd-Price et al., 2019]
12.13-diHOME	[Levan et al., 2019]
Saccharin	[Qin, 2012]
Salicylate	[Caprilli et al., 2009]
Eicosadienoate	[Sitkin and Pokrotnieks, 2018]
Adrenate	[Lloyd-Price et al., 2019]
Hydrocinnamate	[Price et al., 2017]
Caproate	[Le Gall et al., 2011]
Docosapentaenoate	[Solakivi et al., 2011]
Docosahexaenoate	[Solakivi et al., 2011]
Dodecanedioate	[Lee et al., 2017]
Phenyllactate	[Lavelle and Sokol, 2020]
Eicosatrienoate	[Kuroki et al., 1997]
Olmesartan	[Saber et al., 2019]
Taurolithocholate	[Bauset et al., 2021]
Eicosapentaenoate	[Kuroki et al., 1997]
Arachidonate	[Lloyd-Price et al., 2019]
Myristate	[Fretland et al., 1990]
Tetradecanedioate	-
Porphobilinogen	-
Masilinate	-

C Additional Experiments

C.1 Effect of hyperparameters when using sRMMD for knockoff generation

We investigate the effect of the hyperparameters e.g., λ (second-order penalty) and δ (decorrelation penalty) on the performance of our proposed knockoff generation technique. We generate knockoffs using different values of λ and δ , and compute the average FDR and power in a similar way as described in the main paper for each distributional setting. We then observe the FDR vs. power tradeoff to measure the effect of each hyperparameter.

Multivariate Gaussian. Figure 4 shows that for all combinations of λ and δ , generated knockoffs can control the FDR at the prespecified level. Using only sRMMD statistic in the loss function ($\lambda = 0, \delta = 0$) results into low power of detection but better FDR control over the small amplitude region. Adding decorrelation penalty ($\lambda = 0, \delta = 1$) increases both power and FDR level. Knockoffs showcase similar power and FDR control if only the second-order term ($\lambda = 1, \delta = 0$) is added to the loss function. Addition of second-order term and decorrelation penalty ($\lambda = 1, \delta = 1$) marginally improves the power in the lower amplitude region.

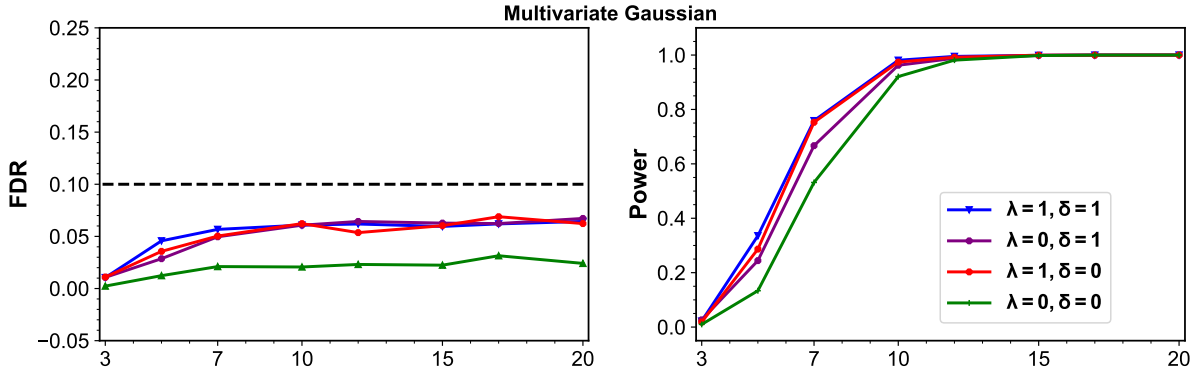


Figure 4: FDR vs amplitude and power vs. amplitude. FDR level is set to 0.1 (black dotted line) for Multivariate Gaussian.

Gaussian Mixture Model. Figure 5 demonstrates that the performance of the proposed method depends on λ and δ in almost similar way as in multivariate Gaussian case (Figure 4). sRMMD statistic ($\lambda = 0, \delta = 0$) can produce knockoffs which have low power but better control of FDR in the smaller amplitude region. Decorrelation penalty ($\lambda = 0, \delta = 1$) increases the power but provides less control of FDR. A better FDR vs. power tradeoff can be achieved by either adding only the second-order term ($\lambda = 1, \delta = 0$) or both ($\lambda = 1, \delta = 1$).

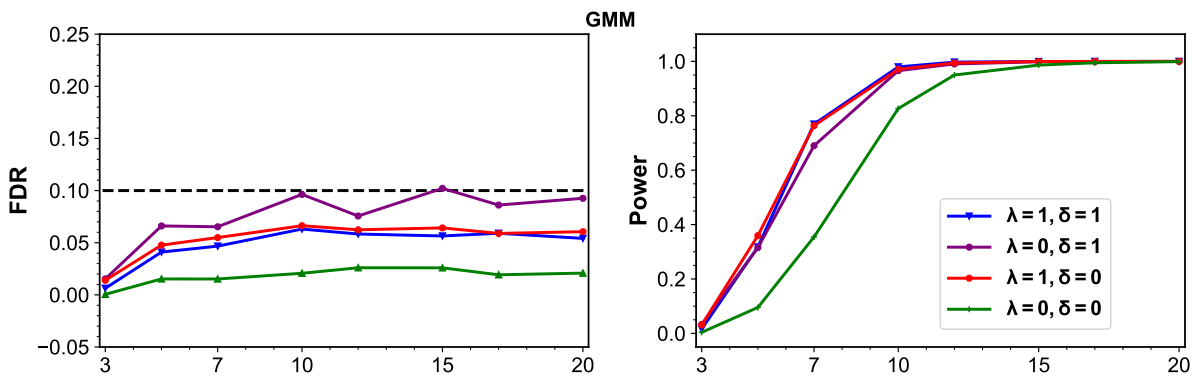


Figure 5: FDR vs amplitude and power vs. amplitude. FDR level is set to 0.1 (black dotted line) for Gaussian Mixture model.

Multivariate Student's t. Figure 6 indicates that without the second-order term ($\lambda = 0$), knockoffs gain very low power of detection over the entire amplitude region. With the increasing λ , the power increases. However, adding both the second-order term and the decorrelation penalty ($\lambda = 1, \delta = 1$) leads to higher power but no control of FDR. Reducing decorrelation penalty ($\lambda = 1, \delta = 0.1$) increases the control of FDR and consequently achieves better FDR vs. power tradeoff.

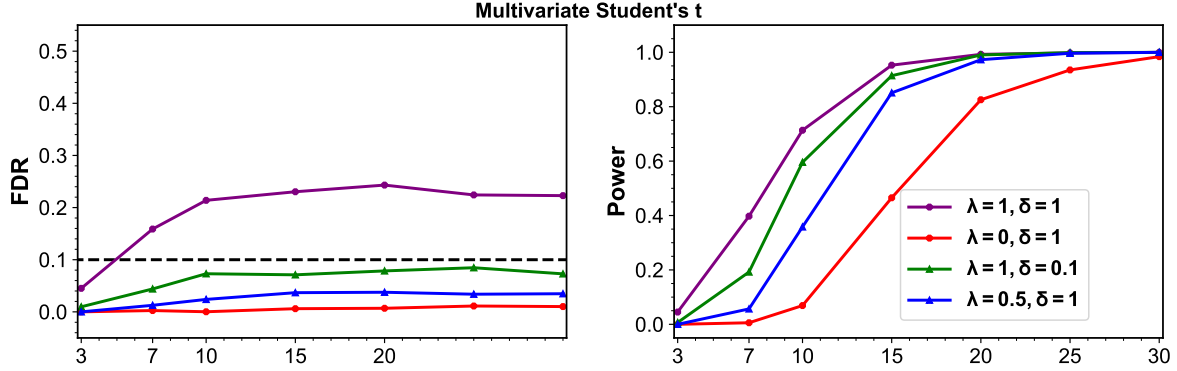


Figure 6: FDR vs amplitude and power vs. amplitude. FDR level is set to 0.1 (black dotted line) for multivariate Student's t distribution.

Sparse Gaussian. From Figure (7), we observe that without the second-order term ($\lambda = 0$), proposed method achieves low power and better control of FDR over the smaller amplitude region. Increasing decorrelation penalty (δ) marginally increases the control of FDR.

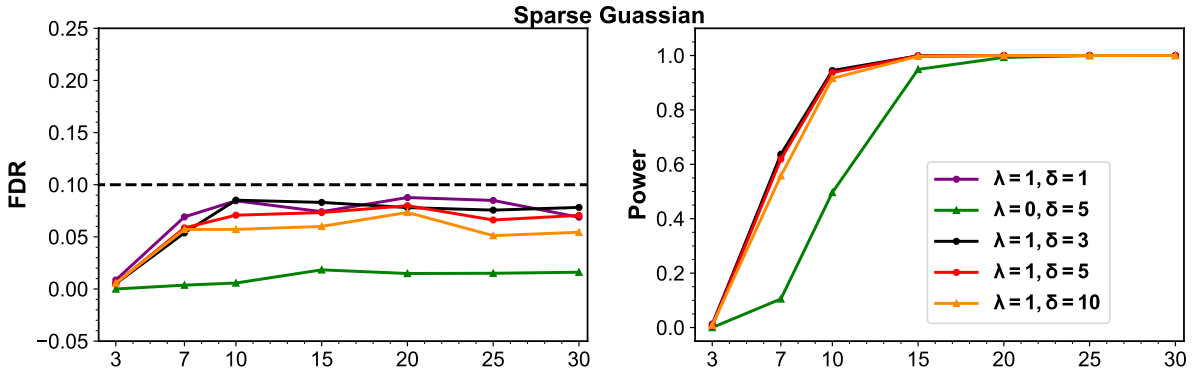


Figure 7: FDR vs amplitude and power vs. amplitude. FDR level is set to 0.1 (black dotted line) for sparse Gaussian distribution.

In summary, it may therefore be said that proposed method of knockoff generation is robust to hyperparameters in terms of FDR control in most cases. However, adding a second-order term or a decorrelation penalty or both can significantly improve the FDR vs. power tradeoff.

C.2 Behavior of the sRE statistic

In this section we investigate the behavior of the sRE statistic w.r.t. the sample size, dimension and entropic regularization parameter. Similar to Section 5.1, we consider two Uniform distributions having bounded supports, $U[0, 1]^d$ and $U[s, s + 1]^d$ and measure sRE for $s \in [-10, 10]$ between them.

Figure 8 shows the scaled sRE statistic for different combinations of sample size n , dimension d and entropy regularizer ε . sRE with $\varepsilon = 0$ (dubbed as RE) saturates to the constant maximum for all combinations of n and d over the region where the supports of the two distributions are completely disjoint. With $\varepsilon = 1$, sRE does not saturate when d is small, but with increasing d , it shows similar behavior as RE. As one can see from the plots that, for increasing d , this saturation can be prevented by using larger ε and larger sample size n .

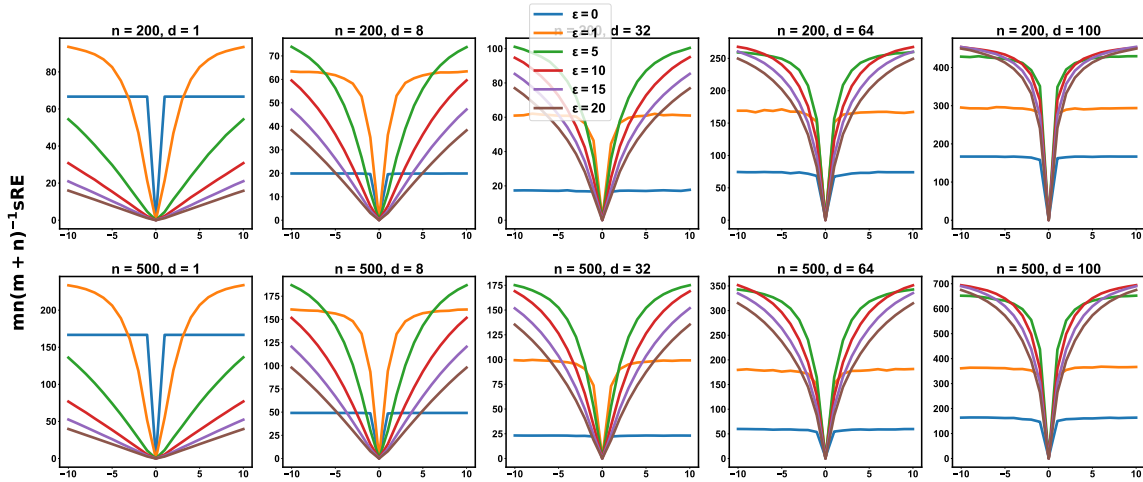


Figure 8: Scaled $\text{RE}(\varepsilon = 0)$ and sRE (y-axis) between two uniform distributions with bounded supports. n and d denote the number of samples and dimension. RE achieves a constant maximum in the region, where the two supports are completely disjoint, for all n, d . sRE do not saturate for increased d if ε and n is larger.

Comparing the plot of sRMMD statistic (Figure 1, main body), we observe that both sRE and sRMMD statistics behave in a very similar way w.r.t. n, d and ε . It may therefore be said that, the behavior of these statistics depends on how the ranks and the soft ranks are defined.

C.3 Use of sRE in learning a generative model

In this section, we validate the use of sRE statistic as a loss function. We use a similar generative model architecture as described in [Li et al., 2015] and instead of using maximum mean discrepancy (MMD) [Gretton et al., 2012], we use sRE as the loss. As recommended, we employ an Autoencoder [Kingma and Welling, 2013] to project the data into a latent space of reduced dimension. We set the latent space dimension equal to $d = 8$. We train this model with Adam optimizer [Kingma and Ba, 2014] with the batch size 256 and the learning rate 0.001.

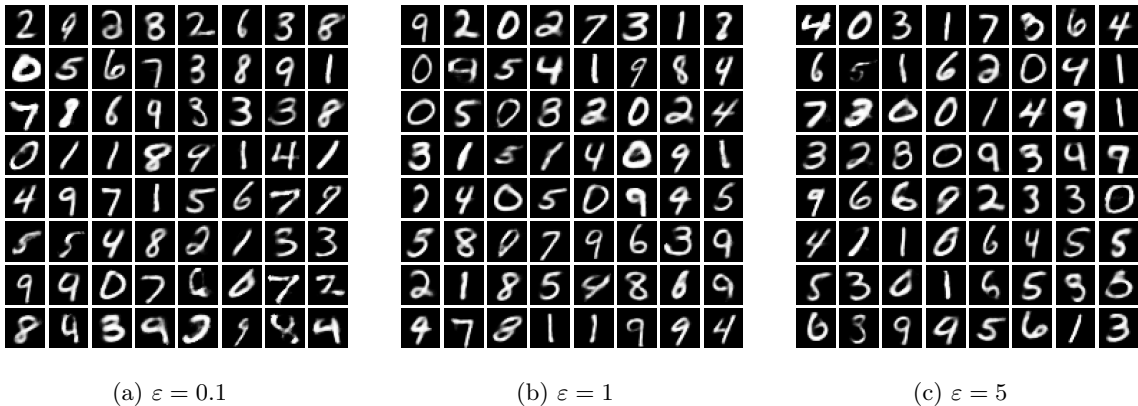


Figure 9: MNIST image generation using sRE based generative model.

Figure 9 shows the MNIST image generated using sRE statistic with $\varepsilon = 0.1, 1, 5$. Though Figure 8 shows the saturation behavior of sRE statistic with smaller ε when d is large, which is undesirable in learning a generative model, the use of Autoencoder facilitates the generation of valid digits with smaller ε . In addition, this sRE based generative model can produce unambiguous digits with $\varepsilon = 1, 5$ with less computational and sample complexity [Mena and Niles-Weed, 2019] compared to using smaller $\varepsilon = 0.1$.